



Science Arts & Métiers (SAM)

is an open access repository that collects the work of Arts et Métiers Institute of Technology researchers and makes it freely available over the web where possible.

This is an author-deposited version published in: <https://sam.ensam.eu>
Handle ID: <http://hdl.handle.net/10985/24702>

To cite this version :

Xiulin WANG, Jinlin GONG, Youxi HUANG, Eric SEMAIL, Ngac Ky NGUYEN, Ling PENG - High Quality Sensorless Control Strategy for Seven-phase PMSM in Full Speed Range - In: 2023 26th International Conference on Electrical Machines and Systems (ICEMS), Chine, 2023-11-05 - 2023 26th International Conference on Electrical Machines and Systems (ICEMS) - 2023

Any correspondence concerning this service should be sent to the repository

Administrator : scienceouverte@ensam.eu



High Quality Sensorless Control Strategy for Seven-phase PMSM in Full Speed Range

Xiulin Wang
School of Electrical Engineering
Shandong University
Jinan, China
wxl17375874516@163.com

Jinlin Gong
School of Electrical Engineering
Shandong University
Jinan, China
gongjinlin@sdu.edu.cn

Youxi Huang
Laboratory of Electrical Engineering
and Power Electronics of Lille
Arts et Métiers
Lille, France
1020469633@qq.com

Eric Semail
Laboratory of Electrical Engineering
and Power Electronics of Lille
Arts et Métiers
Lille, France
eric.semail@ensam.eu

NgacKy Nguyen
Laboratory of Electrical Engineering
and Power Electronics of Lille
Arts et Métiers
Lille, France
ngacky.nguyen@ensam.eu

Ling Peng
Wuhan Institute of Marine Electric
Propulsion
Wuhan, China
pengling.2001@tsinghua.org.cn

Abstract—At low speed, the traditional high frequency signal injection (HFSI) control strategy will lead to large torque ripple, and affect the estimation accuracy of the position/speed related to sensorless control algorithm, and finally lead to the problem of the system stability. Based on the characteristics of seven-phase Permanent Magnet Synchronous Machine (PMSM), this paper proposes a new sensorless control strategy in full speed range. In the zero/low speed range, HFSI method is applied to the 5th harmonic subspace, which reduce the torque ripple of the machine.. In the medium/high speed range, the sliding mode observer (SMO) is used in the 1st harmonic subspace to estimate the speed and position of the machine. The influences between the two methods are effectively reduced when exchanging from zero/low speed to medium/high speed range. Moreover, the estimated position and speed is more accurate and the torque ripple is smaller with the proposed sensorless control strategy. Finally, the effectiveness of the proposed strategy is verified by simulation results.

Keywords—Seven-phase Machine, Sliding Mode Observer, High-Frequency Signal Injection, Full Speed Range

I. INTRODUCTION

In recent years, PMSM have been widely used due to simple structure, high power density, high efficiency and high reliability[1]. The high-performance drive control system of PMSM usually needs to install a position sensor on the rotor shaft to obtain accurate position and speed information to achieve high quality control. However, in practical applications, the use of position sensors will lead to the following problems: the installation is difficult, the system cost increases, the system volume increases and the complex environment limites [2]. Therefore, in order to resolve these problems caused by position sensors, the research of sensorless control has attracted more and more attention.

At present, the sensorless control method of PMSM is mainly divided into two types: The first method is to inject the high-frequency voltage signal into the PMSM, and estimate the position and speed by analyzing the high-frequency current signal obtained by the current sensor. This method is suitable for zero/low speed range, i.e. the back EMF of the machine is small[3]. The second method is to estimate the back EMF of the machine, and then analyze the position and speed signals. This method is suitable for medium/high speed range, including Extended Kalman Filter (EKF)[4][5], Model Reference Adaptive (MRA)[6] and SMO[7]. Compared with

other observer algorithms, SMO has the advantages of simple parameter design and strong robustness, and is widely used in sensorless control systems[8].

Compared with the traditional three-phase PMSM, multi-phase PMSM has the advantages of high fault tolerance and low torque ripple[9]. The sensorless control methods of multiphase pmsm are similar to that of three-phase machine, but the algorithm itself has particularity. According to the characteristics of five-phase PMSM, HFSI is applied to the third harmonic subspace, which reduces the torque ripple of the machine[10]. For the third harmonic current in the five-phase PMSM, the SMO considering the third harmonic current is designed in the middle and high speed operation stage[11]. The SMO is combined with an adaptive band-pass filter to estimate the position and velocity signals[12].

Based on the characteristics of seven-phase PMSM, this paper proposes a new sensorless control strategy in full speed range, t.i.e., HFSI is applied to the 5th harmonic subspace in the zero/low speed range, and SMO is used in the medium/high speed domain. Compared to the traditional sensorless control strategy, the proposed strategy can effectively reduce the torque ripples of the machine in the zero-low speed domain and improve the estimation accuracy of the position/speed, and thus the high quality of sensorless control can be achieved in the full speed range.

A. Voltage equation in α - β coordinate system

The salient pole effects of the used machine in this paper is very small, which can be approximated as a non-salient pole machine. In the stationary coordinate system, the voltage equation of the seven-phase PMSM in the fundamental space is as follows :

$$\begin{bmatrix} u_{\alpha 1} \\ u_{\beta 1} \end{bmatrix} = \begin{bmatrix} R + L_1 \frac{d}{dt} & 0 \\ 0 & R + L_1 \frac{d}{dt} \end{bmatrix} \begin{bmatrix} i_{\alpha 1} \\ i_{\beta 1} \end{bmatrix} + \begin{bmatrix} E_{\alpha} \\ E_{\beta} \end{bmatrix} \quad (1)$$

where $u_{\alpha 1}$, $u_{\beta 1}$ are stator voltage, $i_{\alpha 1}$, $i_{\beta 1}$ are stator current, $E_{\alpha 1}$, $E_{\beta 1}$ are emfs, R is stator resistance, L_1 is stator inductance.

The above variables and parameters are in the fundamental space. And, the expression of $E_{\alpha 1}$, $E_{\beta 1}$ is:

$$\begin{bmatrix} E_{\alpha 1} \\ E_{\beta 1} \end{bmatrix} = \omega \psi_f \begin{bmatrix} -\sin \theta \\ \cos \theta \end{bmatrix} \quad (2)$$

where ω is the electrical angular velocity of rotor, ψ_f is permanent magnet flux linkage, θ is position of rotor.

B. Voltage equation in d - q coordinate system

In synchronous rotating coordinate system, the voltage equations of the seven-phase PMSM in the fundamental space and the 5th harmonic subspace are as follows:

$$\begin{bmatrix} u_{d1} \\ u_{q1} \end{bmatrix} = \begin{bmatrix} R + L_{d1} \frac{d}{dt} & 0 \\ 0 & R + L_{q1} \frac{d}{dt} \end{bmatrix} \begin{bmatrix} i_{d1} \\ i_{q1} \end{bmatrix} + \omega \begin{bmatrix} -L_{q1} i_{q1} \\ L_{d1} i_{d1} + \psi_{m1} \end{bmatrix} \quad (3)$$

$$\begin{bmatrix} u_{d5} \\ u_{q5} \end{bmatrix} = \begin{bmatrix} R + L_{d5} \frac{d}{dt} & 0 \\ 0 & R + L_{q5} \frac{d}{dt} \end{bmatrix} \begin{bmatrix} i_{d5} \\ i_{q5} \end{bmatrix} + 5\omega \begin{bmatrix} -L_{q5} i_{q5} \\ L_{d5} i_{d5} + \psi_{m5} \end{bmatrix} \quad (4)$$

where u_{d1} , u_{q1} , u_{d5} , u_{q5} are stator voltage, i_{d1} , i_{q1} , i_{d5} , i_{q5} are stator current, ψ_{m1} , ψ_{m5} are permanent magnet flux amplitude, L_{d1} , L_{d5} is direct axis inductance, L_{q1} , L_{q5} is quadrature axis inductance. Here, u_{d1} , u_{q1} , i_{d1} , i_{q1} , ψ_{m1} , L_{d1} , L_{q1} are in the fundamental space, u_{d5} , u_{q5} , i_{d5} , i_{q5} , ψ_{m5} , L_{d5} , L_{q5} are in the 5th harmonic subspace.

III. SENSORLESS CONTROL IN ZERO-LOW SPEED RANGE

In the zero/low speed range, this paper uses HFSI to estimate the speed and position of the rotor. The HFSI proposed in this paper injects a high-frequency sinusoidal voltage signal in the direct axis, which can make the machine produce a saturated salient pole effect, so this method can be applied to the non-salient pole machine.

In the synchronous rotating coordinate system, the high-frequency voltage equations of the seven-phase permanent magnet synchronous machine in the fundamental space and the fifth harmonic subspace are as follows :

$$\begin{bmatrix} u_{dh1} \\ u_{qh1} \end{bmatrix} = R \begin{bmatrix} i_{dh1} \\ i_{qh1} \end{bmatrix} + \frac{d}{dt} \begin{bmatrix} L_{d1} i_{dh1} \\ L_{q1} i_{qh1} \end{bmatrix} + \omega \begin{bmatrix} -L_{q1} i_{qh1} \\ L_{d1} i_{dh1} + \psi_{m1} \end{bmatrix} \quad (5)$$

$$\begin{bmatrix} u_{dh5} \\ u_{qh5} \end{bmatrix} = R \begin{bmatrix} i_{dh5} \\ i_{qh5} \end{bmatrix} + \frac{d}{dt} \begin{bmatrix} L_{d5} i_{dh5} \\ L_{q5} i_{qh5} \end{bmatrix} + 5\omega \begin{bmatrix} -L_{q5} i_{qh5} \\ L_{d5} i_{dh5} + \psi_{m5} \end{bmatrix} \quad (6)$$

where u_{dh1} , u_{qh1} , u_{dh5} , u_{qh5} are high-frequency voltage, i_{dh1} , i_{qh1} , i_{dh5} , i_{qh5} are high-frequency current. Here, u_{dh1} , u_{qh1} , i_{dh1} , i_{qh1} are in the fundamental space, u_{dh5} , u_{qh5} , i_{dh5} , i_{qh5} are in the 5th harmonic subspace.

In (5) and (6), the voltage equation can be divided into three parts from left to right: resistance voltage term, inductance voltage term and back EMF term. When injecting HF signal, the inductance voltage is much larger than the resistance voltage. And because the ω is small, the back EMF term is much smaller than the inductance voltage. Therefore, the resistance voltage term and the back EMF term can be ignored. The simplified high frequency voltage equation is as follows :

$$\begin{bmatrix} u_{dh1} \\ u_{qh1} \end{bmatrix} = \begin{bmatrix} L_{d1} & 0 \\ 0 & L_{q1} \end{bmatrix} \frac{d}{dt} \begin{bmatrix} i_{dh1} \\ i_{qh1} \end{bmatrix} \quad (7)$$

$$\begin{bmatrix} u_{dh5} \\ u_{qh5} \end{bmatrix} = \begin{bmatrix} L_{d5} & 0 \\ 0 & L_{q5} \end{bmatrix} \frac{d}{dt} \begin{bmatrix} i_{dh5} \\ i_{qh5} \end{bmatrix} \quad (8)$$

A. HFSI in Fundamental Space

Fig. 1 shows the relationship between estimated coordinate system ($\hat{d}_1 - \hat{q}_1$) and actual coordinate system ($d_1 - q_1$) in fundamental space. Here, θ_{err} is the error of the estimated position.

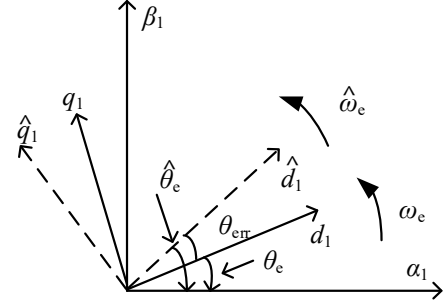


Fig. 1. The coordinate system in the fundamental space

Firstly, a high-frequency voltage signal is injected into the \hat{d}_1 axis of the estimated coordinate system:

$$\begin{bmatrix} \hat{u}_{dh1} \\ \hat{u}_{qh1} \end{bmatrix} = \begin{bmatrix} u_{inj} \cos \omega_h t \\ 0 \end{bmatrix} \quad (9)$$

where u_{inj} is the amplitude of the injected high-frequency voltage, ω_h is the angular frequency of the injected high-frequency voltage.

According to the positional relationship between estimated and actual coordinate systems, the high frequency voltage signal in the d_1 - q_1 coordinate system can be expressed as:

$$\begin{bmatrix} u_{dh1} \\ u_{qh1} \end{bmatrix} = \begin{bmatrix} \hat{u}_{dh1} \times \cos \theta_{err} \\ \hat{u}_{qh1} \times \sin \theta_{err} \end{bmatrix} \quad (10)$$

According to (7) (9) (10), the high-frequency current on the \hat{q}_1 axis can be expressed as :

$$\hat{i}_{qh1} = \frac{u_{inj} \sin \omega_h t}{2\omega_h L_d L_q} (L_{q1} - L_{d1}) \sin 2\theta_{err} \quad (11)$$

The current is then demodulated, i.e., multiplied by $\sin(\omega_h t)$. By using A low-pass filter (LPF) the error signal ε_1 containing the rotor position angle information can be obtained as follows:

$$\varepsilon_1 = \text{LPF}(\hat{i}_{qh1} \sin \omega_h t) = \frac{u_{inj} (L_{q1} - L_{d1})}{4\omega_h L_d L_{q1}} \sin 2\theta_{err} \quad (12)$$

Fig. 2 shows the control block diagram of HFSI in the fundamental space. When θ_{err} is zero, ε_1 is also zero, so the position and speed of the rotor can be obtained through the phase-locked loop (PLL).

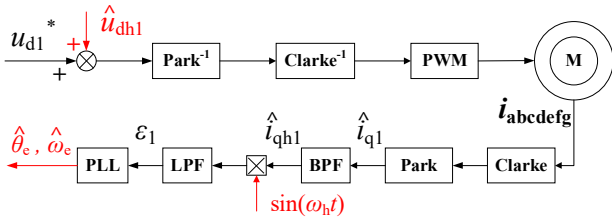


Fig. 2. HFSI in the fundamental space

B. HFSI in 5th Harmonic Subspace

Fig. 3 shows the relationship between estimated coordinate system ($\hat{d}_5 - \hat{q}_5$) and actual coordinate system ($d_5 - q_5$) in the 5th harmonic subspace.

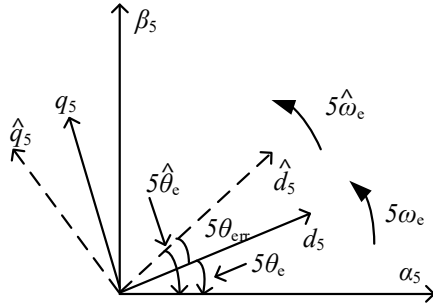


Fig. 3. The coordinate system in the 5th harmonic subspace

Firstly, a high-frequency voltage signal is injected into the \hat{d}_5 axis of the estimated coordinate system:

$$\begin{bmatrix} \hat{u}_{dh5} \\ \hat{u}_{qh5} \end{bmatrix} = \begin{bmatrix} u_{inj} \cos \omega_h t \\ 0 \end{bmatrix} \quad (13)$$

The derivation process of \hat{i}_{qh5} is the same as that of \hat{i}_{qh1} .

The expression of current \hat{i}_{qh5} is as follows :

$$\hat{i}_{qh5} = \frac{u_{inj} \sin \omega_h t}{2\omega_h L_{d5} L_{q5}} (L_{q5} - L_{d5}) \sin 10\theta_{err} \quad (14)$$

After demodulation and filtering, the error signal ε_5 containing the rotor position angle information can be obtained as follows:

$$\varepsilon_5 = LPF(\hat{i}_{qh5} \sin \omega_h t) = \frac{u_{inj} (L_{q5} - L_{d5})}{4\omega_h L_{d5} L_{q5}} \sin 10\theta_{err} \quad (15)$$

Fig. 4 shows the control block diagram of HFSI in the 5th harmonic subspace. When θ_{err} is zero, ε_5 is also zero, so the position and speed of the rotor can be obtained through the PLL.

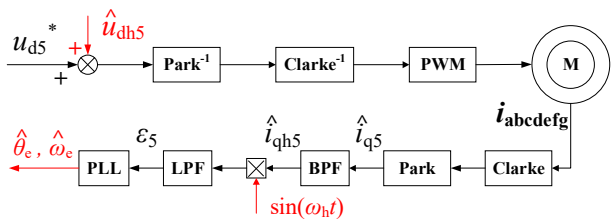


Fig. 4. HFSI in the 5th harmonic subspace

C. Advantages of HFSI in 5th harmonic subspace

The flux linkage and the back-EMF waveforms and the Fourier decompositions of the seven-phase PMSM are shown in Fig. 5 and Fig. 6, respectively [13].

Since the flux linkage and back EMF of the 5th harmonic subspace are of very small value, i.e. close to be zero, the amplitude of the high-frequency torque ripples generated by injecting high-frequency voltage signals into the 5th harmonic subspace will be much smaller than the one in the fundamental subspace.

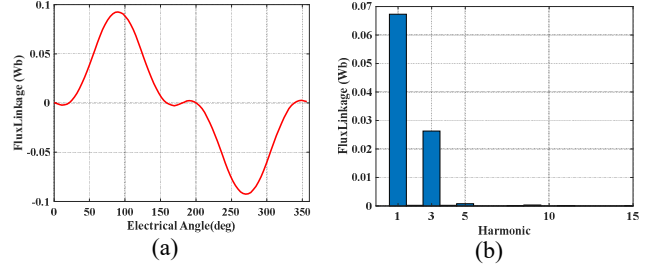


Fig. 5. Flux linkage waveform

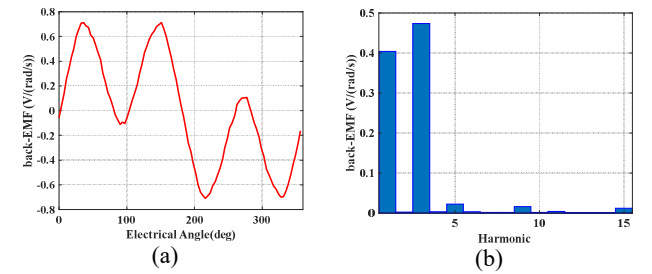


Fig. 6. Back-EMF waveform

IV. SENSORLESS CONTROL IN FULL SPEED RANGE

A. Sensorless control in medium-high speed range

In the medium/high speed range, SMO is used to estimate the speed and position of the rotor. Substituting (1) to the current state equation as follows :

$$\frac{d}{dt} \begin{bmatrix} i_{\alpha 1} \\ i_{\beta 1} \end{bmatrix} = -\frac{R}{L_1} \begin{bmatrix} i_{\alpha 1} \\ i_{\beta 1} \end{bmatrix} + \frac{1}{L_1} \begin{bmatrix} u_{\alpha 1} \\ u_{\beta 1} \end{bmatrix} - \frac{1}{L_1} \begin{bmatrix} E_{\alpha 1} \\ E_{\beta 1} \end{bmatrix} \quad (16)$$

In order to estimate the position and speed of the machine, the SMO is constructed as follows:

$$\frac{d}{dt} \begin{bmatrix} \hat{i}_{\alpha 1} \\ \hat{i}_{\beta 1} \end{bmatrix} = -\frac{R}{L_1} \begin{bmatrix} \hat{i}_{\alpha 1} \\ \hat{i}_{\beta 1} \end{bmatrix} + \frac{1}{L_1} \begin{bmatrix} u_{\alpha 1} \\ u_{\beta 1} \end{bmatrix} - \frac{1}{L_1} \begin{bmatrix} u_{smo\alpha 1} \\ u_{smo\beta 1} \end{bmatrix} \quad (17)$$

where $\hat{i}_{\alpha 1}, \hat{i}_{\beta 1}$ are the estimated currents, $u_{smo\alpha 1}, u_{smo\beta 1}$ are the sliding mode control functions.

The current error equation is obtained by (16) and (17).

$$\frac{d}{dt} \begin{bmatrix} \tilde{i}_{\alpha 1} \\ \tilde{i}_{\beta 1} \end{bmatrix} = -\frac{R}{L_1} \begin{bmatrix} \tilde{i}_{\alpha 1} \\ \tilde{i}_{\beta 1} \end{bmatrix} + \frac{1}{L_1} \begin{bmatrix} E_{\alpha 1} \\ E_{\beta 1} \end{bmatrix} - \frac{1}{L_1} \begin{bmatrix} u_{smo\alpha 1} \\ u_{smo\beta 1} \end{bmatrix} \quad (18)$$

The sliding mode surface and sliding mode control function are designed in (19) (20).

$$s = \begin{bmatrix} s_{\alpha 1} \\ s_{\beta 1} \end{bmatrix} = \begin{bmatrix} \tilde{i}_{\alpha 1} \\ \tilde{i}_{\beta 1} \end{bmatrix} = \begin{bmatrix} i_{\alpha 1} - \hat{i}_{\alpha 1} \\ i_{\beta 1} - \hat{i}_{\beta 1} \end{bmatrix} \quad (19)$$

$$\begin{bmatrix} u_{smo\alpha 1} \\ u_{smo\beta 1} \end{bmatrix} = k_{sild} \times \begin{bmatrix} \text{sat}(\tilde{i}_{\alpha 1}) \\ \text{sat}(\tilde{i}_{\beta 1}) \end{bmatrix} \quad (20)$$

where s_{α} and s_{β} are the sliding mode surfaces, k_{sild} is the gain coefficient.

When the state variables are on the sliding surface, the s and the derivation of s are zero, and $E_{\alpha 1} = u_{smo\alpha 1}$, $E_{\beta 1} = u_{smo\beta 1}$.

Finally, the speed and position of the machine can be obtained by PLL. Fig. 7 shows the control block diagram of SMO in the fundamental space.

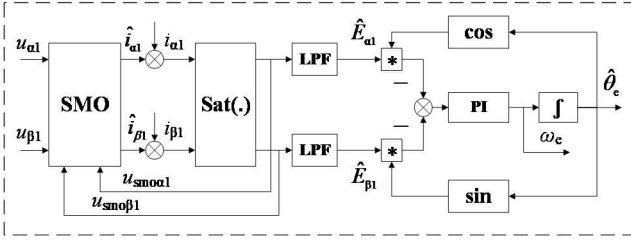


Fig. 7. SMO in the fundamental space

B. Control Strategy in Full Speed Range

Fig. 8 shows the two control strategies in full speed range, which are compared in this paper. At zero/low speed range, strategy 1 employs the HFSI in the fundamental space (HFSI-1), and strategy 2 employs the HFSI in the 5th harmonic subspaces (HFSI-5). At medium/high speed range, the SMO is both used in the two strategies. This paper adopts the hysteresis switching algorithm, in order to avoid the problem of repeated switching when the speed variate from low to high or inverse versa. When the machine accelerates, the switching speed is set to n_{up} . When the machine decelerates, the switching speed is set to n_{down} .

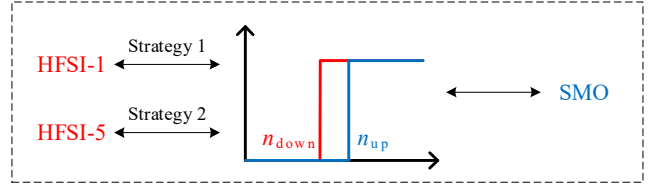


Fig. 8. control strategy in full speed range

In the $[n_{down}, n_{up}]$ speed range, the HFSI and the SMO algorithms are used simultaneously. In strategy 1, HFSI-1 will affect the estimation of SMO, because HFSI-1 injects high-frequency voltage into the fundamental space and generates high-frequency current. Strategy 2 can avoid this problem, thanks to the injection of the high-frequency voltage is done in the 5th harmonic space, which will not affect the use of SMO. Moreover, according to the previous analysis, in the zero-low speed range, the high-frequency torque ripple generated by strategy 2 will be much smaller than that generated by strategy 1. The advantages of the strategy 2 shown above are furtherly studied and validated through the simulations in the following part.

V. SIMULATION RESULTS

In order to verify the effectiveness of the proposed strategy, the estimated speed, the estimated position and electromagnetic torque under different sensorless control strategies are compared and analyzed through the simulation by using MATLAB/SIMULINK. Fig. 9 shows the block diagram of seven-phase PMSM sensorless control in the full speed range. The parameters of the seven-phase PMSM used in the simulation are show in TABLE I.

The reference speed of the seven-phase PMSM is set as follows : In 0-1.5s, the speed is increased from 0rpm to 200rpm. In 1.5-3s, the speed is maintained at 200 rpm. In 3-4.5 s, the speed is reduced from 200 rpm to 50 rpm. In 4.5-6s, the speed is maintained at 50 rpm. The parameters of hysteresis switching algorithm : n_{up} is set to 100rpm, and n_{down} is set to 80rpm. The load of the machine is set to 1.5 Nm.

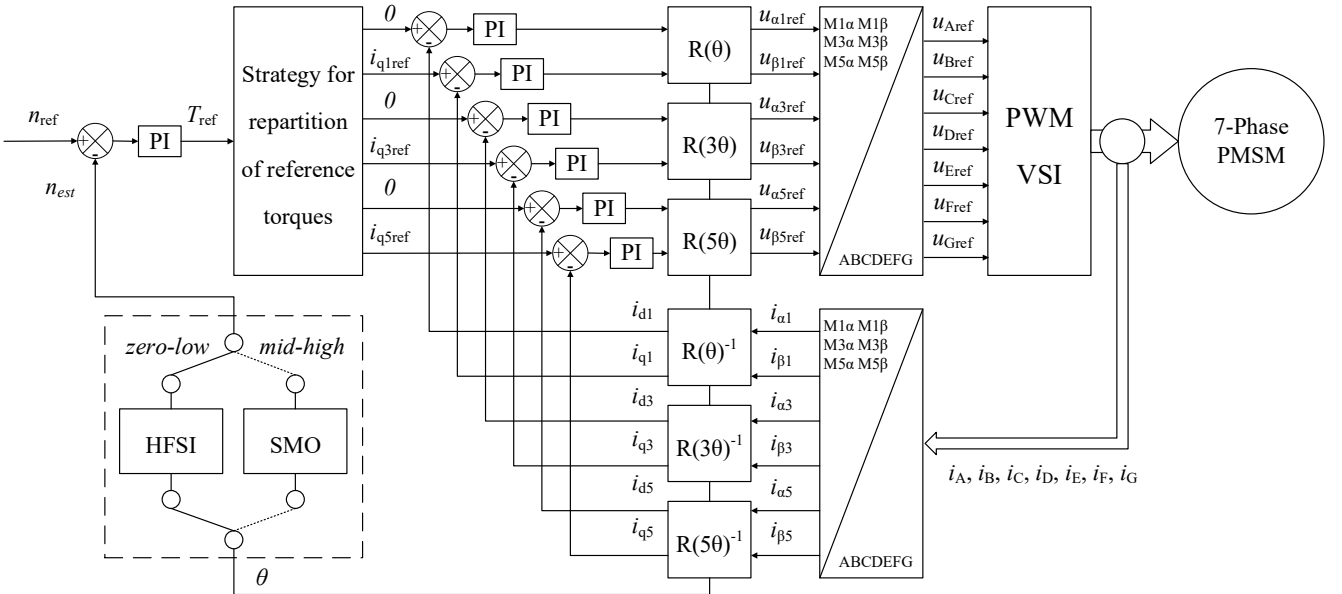


Fig. 9. The block diagram of seven-phase PMSM sensorless control in full speed range

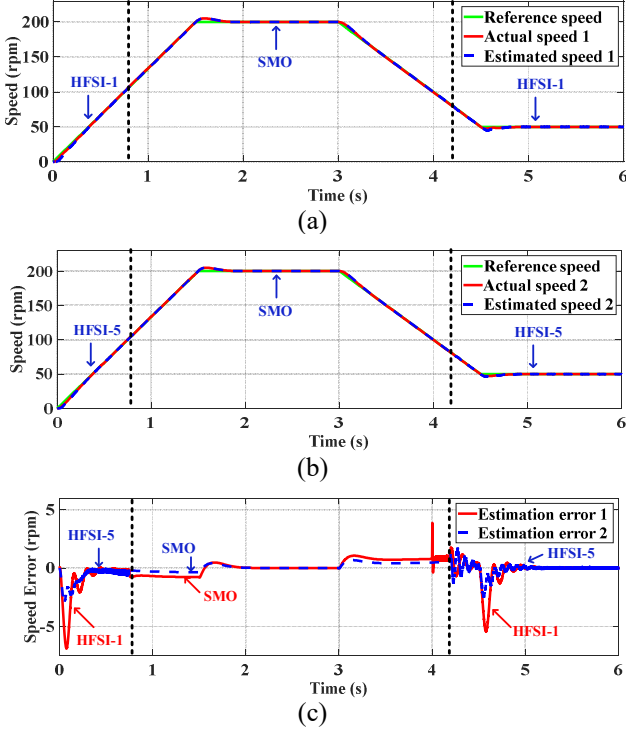


Fig. 10. (a) Actual and estimated speed of strategy1 (b) Actual and estimated speed of strategy2 (c) Speed estimation error

Fig. 10 shows the tracking of machine speed under different control strategies. From Fig. 10 (a) (b), it can be seen that the estimated speed of strategy 1 and strategy 2 can both well track the actual speed. According to Fig. 10 (c), the maximum speed estimation error of strategy 1 is 9rpm, and that of strategy 2 is 3rpm, which is decreased more than 60%.

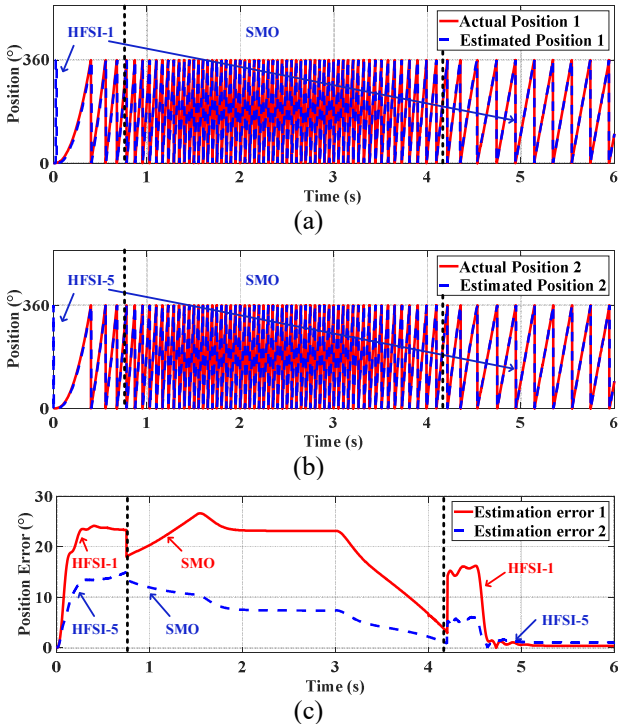


Fig. 11. (a) Actual and estimated position of strategy1 (b) Actual and estimated position of strategy2 (c) Position estimation error

Fig. 11 shows the position tracking of the rotor under different control strategies. From Fig. 11 (a) (b), it can be seen that the estimated position of strategy 1 and strategy 2 can both well track the rotor position. It can be seen from Fig. 11 (c) that the estimated position error of strategy 2 is decreased about 50%.

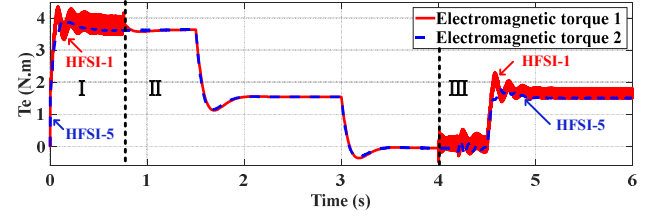


Fig. 12. Electromagnetic torque of seven-phase PMSM

Fig. 12 shows the electromagnetic torque of seven-phase PMSM with different control strategies. In the intervals I and III, high-frequency voltage signals are injected into the machine. In interval II, there is no high-frequency voltage signal injected into the machine. It can be seen that when a high-frequency voltage signal is injected into the machine, the torque ripple can be effectively reduced by using the strategy 2.

Through the above simulation results, it can be concluded that both strategy 1 and strategy 2 can achieve sensorless control of seven-phase PMSM in the full speed range. However, compared to the strategy 1, the strategy 2 performs better in terms of the estimation accuracy of speed and position, and the reduction of the torque ripples.

TABLE I. PARAMETERS OF THE SEVEN-PHASE PMSM

Parameter	Value	Unit
R (stator resistance)	0.67	Ω
L (stator inductance)	3.27	mH
P (pole-pairs)	6	
J (moment of inertia)	0.1	kg m^2
Ψ_n (flux linkage in fundamental space)	0.068	Wb
Ψ_B (flux linkage in 3 th harmonic subspace)	0.026	Wb

VI. CONCLUSION

In this paper, based on the particularity of seven-phase PMSM machine, a new sensorless control strategy in full speed range is proposed. Compared to the traditional sensorless control strategy, the new strategy injects the high-frequency voltage signal in the 5th harmonic subspace instead of the fundamental one. Using the new sensorless control strategy, the high-frequency torque ripples can be reduced to almost zero. The accuracy of the speed and the position estimation can be improved by 150% and 100%, respectively.

REFERENCES

- [1] T. Wang, B. Wang, Y. Yu and D. Xu, "High-Order Sliding-Mode Observer With Adaptive Gain for Sensorless Induction Motor Drives in the Wide-Speed Range," in IEEE Transactions on Industrial Electronics, vol. 70, no. 11, pp. 11055-11066, Nov. 2023.
- [2] D. Wen, W. Wang, Y. Zhang, "Sensorless Control of Permanent Magnet Synchronous Motor in Full Speed Range", Chinese Journal of Electrical Engineering, Vol.8, No.2, pp.97-107, 2022.
- [3] J. Zhou and J. Liu, "An Improved High Frequency Square Wave Injection Permanent Magnet Synchronous Motor sensorless Control,"

2021 6th International Conference on Control and Robotics Engineering (ICCRE), Beijing, China, 2021, pp. 101-105.

- [4] E. Zerdali and M. Barut, "The Comparisons of Optimized Extended Kalman Filters for Speed-Sensorless Control of Induction Motors," in *IEEE Transactions on Industrial Electronics*, vol. 64, no. 6, pp. 4340-4351, June 2017.
- [5] M. S. Termizi, J. M. Lazi, Z. Ibrahim, M. H. N. Talib, M. J. A. Aziz and S. M. Ayob, "Sensorless PMSM drives using Extended Kalman Filter (EKF)," 2017 IEEE Conference on Energy Conversion (CENCON), Kuala Lumpur, Malaysia, 2017, pp. 145-150.
- [6] T. Orlowska-Kowalska and M. Dybkowski, "Stator-Current-Based MRAS Estimator for a Wide Range Speed-Sensorless Induction-Motor Drive," in *IEEE Transactions on Industrial Electronics*, vol. 57, no. 4, pp. 1296-1308, April 2010.
- [7] W. Zhu, S. Li, H. Du and X. Yu, "Nonsmooth Observer-Based Sensorless Speed Control for Permanent Magnet Synchronous Motor," in *IEEE Transactions on Industrial Electronics*, vol. 69, no. 12, pp. 13514-13523, Dec. 2022.
- [8] T. Wang, B. Wang, Y. Yu and D. Xu, "Discrete Sliding-Mode-Based MRAS for Speed-Sensorless Induction Motor Drives in the High-Speed Range," in *IEEE Transactions on Power Electronics*, vol. 38, no. 5, pp. 5777-5790, May 2023.
- [9] S. Rubino, O. Dordevic, E. Armando, I. R. Bojoi and E. Levi, "A Novel Matrix Transformation for Decoupled Control of Modular Multiphase PMSM Drives," in *IEEE Transactions on Power Electronics*, vol. 36, no. 7, pp. 8088-8101, July 2021.
- [10] G. Liu, C. Geng and Q. Chen, "Sensorless Control for Five-Phase IPMSM Drives by Injecting HF Square-Wave Voltage Signal into Third Harmonic Space," in *IEEE Access*, vol. 8, pp. 69712-69721, 2020.
- [11] A. Hezzi, Y. Bensalem, S. Ben Elghali and M. Naceur Abdelkrim, "Sliding Mode Observer based sensorless control of five phase PMSM in electric vehicle," 2019 19th International Conference on Sciences and Techniques of Automatic Control and Computer Engineering (STA), Sousse, Tunisia, 2019, pp. 530-535.
- [12] D. Semenov, B. Tian, Q. -T. An and L. Sun, "Position estimation for sensorless FOC of five-phase PMSM in electric vehicles," 2016 Australasian Universities Power Engineering Conference (AUPEC), Brisbane, QLD, Australia, 2016, pp. 1-5.
- [13] J. Gong, X. Wang, B. Zhao, F. Tan, E. Semail et al, "Design, Analysis of a Seven-Phase fault-tolerant Bi-Harmonic Permanent Magnet Machine with Three Active Air Gaps for In-Wheel Traction Applications," in *IEEE Transactions on Energy Conversion*, to be appeared.